

Robust $d_{x^2-y^2}$ -wave superconductivity of infinite-layer nickelates

Xianxin Wu,^{1,*} Domenico Di Sante,^{1,†} Tilman Schwemmer,¹ Werner Hanke,¹ Harold Y. Hwang,^{2,3} Srinivas Raghu,^{2,4,‡} and Ronny Thomale^{1,§}

¹*Institut für Theoretische Physik und Astrophysik, Universität Würzburg,
Am Hubland Campus Süd, Würzburg 97074, Germany*

²*Stanford Institute for Materials and Energy Sciences,*

SLAC National Accelerator Laboratory, Menlo Park, California 94025, USA

³*Department of Applied Physics, Stanford University, Stanford, California 94305, USA*

⁴*Department of Physics, Stanford University, Stanford, California 94305, USA*

(Dated: January 3, 2022)

Motivated by the recent observation of superconductivity in strontium doped NdNiO₂, we study the superconducting instabilities in this system from various vantage points. Starting with first-principles calculations, we construct two distinct tight-binding models, a simpler single-orbital as well as a three-orbital model, both of which capture the key low energy degrees of freedom to varying degree of accuracy. We study superconductivity in both models using the random phase approximation (RPA). We then analyze the problem at stronger coupling, and study the dominant pairing instability in the associated t-J model limit. In all instances, the dominant pairing tendency is in the $d_{x^2-y^2}$ channel, analogous to the cuprate superconductors.

Introduction – The observation of superconductivity in the infinite-layer nickelate Nd_{1-x}Sr_xNiO₂ [1] resurrects some of the perennial questions in the field of unconventional superconductivity of the cuprates and related materials [2, 3]. As nickel substitutes for copper in this system, the low energy manifold consists primarily of the Ni-O plane. Therefore, we are invited to revisit whether copper itself is important for the superconductivity exhibited by the cuprates [4–9]. Furthermore, to date, magnetism has not been observed in the parent NdNiO₂ compound [10, 11]. One may therefore question the extent to which close proximity to long-range antiferromagnetism is an essential ingredient in cuprate superconductivity.

To help address these questions, we have studied superconductivity from repulsive interactions in Nd_{1-x}Sr_xNiO₂, adopting both weak- and strong-coupling approaches. Starting with a first-principles study of NdNiO₂, and treating the effects of strontium doping as a rigid shift to the chemical potential, we have obtained tight-binding fits to the electronic structure. As Ni is isoelectronic to copper in this material, it has a d^9 configuration and the low energy physics is dominated by electrons in the Ni- $d_{x^2-y^2}$ orbital (see Fig. 1). There is, however, an additional strong hybridization with the $5d$ orbitals of the rare earth Nd element. As a consequence, there is a non-zero contribution to the low energy physics from the Nd d_{z^2} and d_{xy} orbitals, which acts to introduce some distinction between this system and the infinite layer cuprate material.

However, rather than speculating on the commonalities and differences of the infinite-layer cuprate and nickelate, we have instead chosen to study superconductivity in the nickelate material as a legitimate problem in its own right, one that is independent from the cuprates. The weak-coupling approach, while likely unreliable for normal state properties, does tend to capture the primary property of interest, namely the superconducting ground state itself and, in particular, the symmetry of the superconducting order parameter. We find robust $d_{x^2-y^2}$ -wave superconductivity within the weak-coupling approach. We have obtained this pairing symmetry in two dis-

tinct tight-binding fits to the first-principles calculation, one which is a minimal one-orbital model consisting of the Ni $d_{x^2-y^2}$ orbital, and a more realistic 3-orbital model that includes the d_{z^2} , d_{xy} orbitals of the Nd atom.

In reality, however, the system is likely located at intermediate coupling; it therefore becomes important to analyze the problem from complementary limits. With this in mind, we also analyze the t-J model that results from the limit of strong Ni onsite interactions, and study superconductivity in this model within a mean-field approximation. Such methods led to the conclusion of d -wave pairing in the early days of cuprate physics [12], and we arrive at a similar conclusion in the present context. We also show that with the inclusion of the Nd electron pockets, $d_{x^2-y^2}$ pairing stemming from the effective t-J model is only weakly affected. While these electron pockets ultimately lead to metallic, rather than Mott insulating behavior in the parent compound, their impact on superconductivity appears to be rather weak. The fact that all limits studied here result in $d_{x^2-y^2}$ pairing underlies the robustness of our conclusion.

This Rapid Communication is organized as follows. At first, we present the results of the first-principles computations, where we describe both the minimal single-band and 3-band tight-binding fits to the electronic structure. We then proceed to show our results for the pairing symmetry both in a random phase approximation (RPA) treatment of superconductivity from repulsive interactions, as well as from the analysis of a t-J model description. Both complementary studies are carried out in three dimensions (3D), corresponding to the infinite-layer limit.

First-principles analysis – We performed first-principles calculations within the framework of the density functional theory as implemented in the Vienna ab initio simulation package VASP [13–15]. The generalized gradient approximation, as parametrized by the PBE-GGA functional for the exchange-correlation potential, was used, by expanding the Kohn-Sham wave functions into plane waves up to an energy cutoff of 600

eV and sampling the Brillouin zone on an $16 \times 16 \times 16$ regular mesh [16]. The growth of NdNiO_2 on a SrTiO_3 substrate is simulated by imposing an in-plane lattice constant $a = 3.91 \text{ \AA}$ and relative relaxed out-of-plane parameter $c = 3.37 \text{ \AA}$ [1]. The extraction of the three-orbitals minimal model used to investigate the superconducting tendencies of NdNiO_2 was based on the Wannier functions formalism [17].

Fig. 2 shows the single-particle band structure of NdNiO_2 , along with the orbital contributions relevant for the low-energy model description. Owing to a d^9 electronic configuration in a peculiar +1 oxidation state for Ni, the crystal field imposed by the planar square coordination (Fig. 1) results in a high-lying nominally half-filled $d_{x^2-y^2}$ orbital (red dots), featuring a predominantly two-dimensional character. Nonetheless, the delocalized and formally empty Nd 5d states reside fairly low in energy, leading to a sizable hybridization with Ni 3d bands, and to the appearance of electron pockets at the Γ and $A = (\pi/a, \pi/a, \pi/c)$ (see panel Fig. 2(a)) points. Such pockets mainly display Nd d_{z^2} (yellow squares) and d_{xy} (blue diamonds) orbital contributions, respectively, and determine a concomitant self-doping of the large hole-like Ni $d_{x^2-y^2}$ Fermi surface.

Having established the contribution of the relevant orbitals to the low-energy physics of NdNiO_2 , we consider a three-orbital tight-binding (TB) model which includes long range hopping terms. We introduce the operator $\psi_{\mathbf{k}\sigma}^\dagger = [c_{1\sigma}^\dagger(\mathbf{k}), c_{2\sigma}^\dagger(\mathbf{k}), c_{3\sigma}^\dagger(\mathbf{k})]$, where $c_{\alpha\sigma}^\dagger(\mathbf{k})$ is a fermionic creation operator with σ and α denoting spin and orbital indices, respectively. The orbital index $\alpha = 1, 2, 3$ represents the Nd d_{z^2} for 1, the Nd d_{xy} for 2 and the Ni $d_{x^2-y^2}$ for 3. The tight-binding Hamiltonian can be written as

$$H_{\text{TB}} = \sum_{\mathbf{k}\sigma} \psi_{\mathbf{k}\sigma}^\dagger h(\mathbf{k}) \psi_{\mathbf{k}\sigma}, \quad (1)$$

where $h(\mathbf{k})$ is given in [27], along with the corresponding parameters extracted from a downfolding of the first-principles band structure onto a set of localized Wannier functions. With the above parameters, the obtained band structure fits are given in [27] and reach a good agreement between DFT and

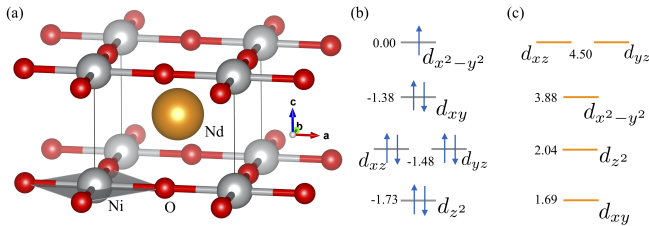


FIG. 1: (a) View of the crystal structure of NdNiO_2 . Ni, O, and Nd atoms are represented by grey, red and orange spheres. The planar coordination in the NiO_2 is highlighted by a grey square. (b) The resulting crystal field is characterized by a top $d_{x^2-y^2}$ orbital, which is singly occupied in a d^9 electronic configuration. (c) Crystal field acting on the formally empty Nd d orbitals. In (b) and (c), the crystal field levels are given in eV, with respect to the Ni $d_{x^2-y^2}$.

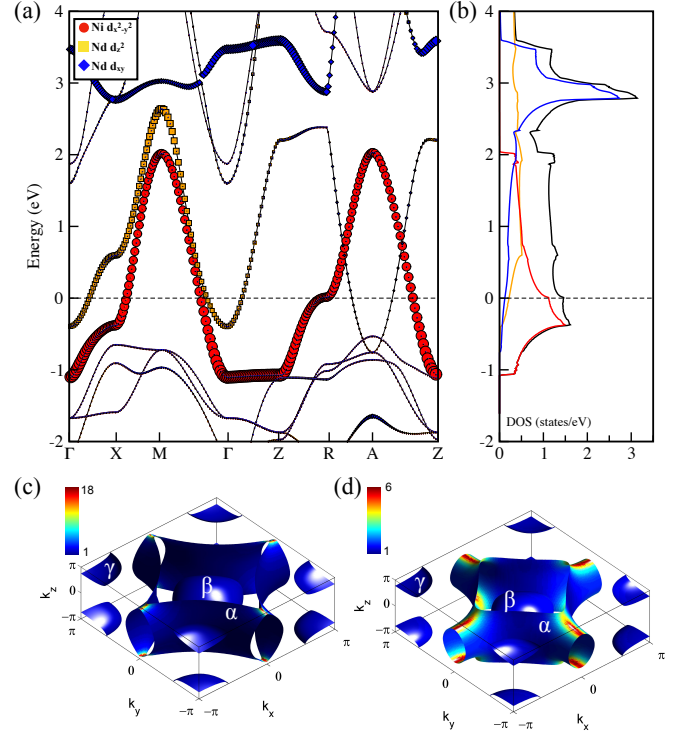


FIG. 2: First-principles band structure (a) and density of states (b) of NdNiO_2 with lattice parameters forced by the commensuration to the SrTiO_3 substrate. The red (Ni $d_{x^2-y^2}$), yellow (Nd d_{z^2}), and blue (Nd d_{xy}) symbols emphasize the relevant orbitals that contribute to the low-energy description. In panel (b) the black curve refers to the sum of the individual contributions. Views of the Fermi surface of NdNiO_2 at (c) pristine filling ($n = 1.0$) and (d) upon 0.2 hole doping ($n = 0.8$). The color scale reports the momentum dependence of the inverse Fermi velocity ($1/v_F(\mathbf{k})$), which is a measure of the DOS. The α Fermi surface displays a van Hove feature evolving from the $k_z = 0$ cut to the $k_z = \pi$ cut, where it changes from a hole pocket around the M point in the $k_z = 0$ plane to an electron pocket around the Z point in the $k_z = \pi$ plane.

the effective TB bands. Near the Fermi level, the DOS is dominantly attributed to the Ni $d_{x^2-y^2}$ orbital, as shown in Fig. 2(b). Further considering the relatively weak interaction effects in the 5d orbitals of Nd, the dominant correlation effects must derive from the 3d $d_{x^2-y^2}$ orbital of Ni in NdNiO_2 . These conclusions are consistent with previous [7, 8] as well as concurrent [18] first principles calculations of this system.

The resulting 3D Fermi surfaces are shown in Fig. 2(c) and (d) for the fillings $n = 1.0$ and $n = 0.8$. For the former case, there is an almost cylindrical, non-dispersive in k_z , hole-like pocket α , and two small electron-like pockets β and γ around the Γ and A points, respectively. With 0.2 hole doping, the electron Fermi surfaces shrink. For the hole pocket, van Hove singularities are reached near the $k_z = \pi$ plane, and its density of states increases considerably along with enhanced nesting, as shown by the red curve in Fig. 2(b). The three-dimensional character of the obtained Fermiology is an essential distinguishing aspect from the infinite-layer

cuprates. Within a weak-coupling framework of superconductivity, such enhancement of the density of states available for pairing as obtained for hole doping in the nickelates typically results in a concomitant increase of the superconducting temperature. The largest contribution to the density of states arises from the large non- k_z -dispersive Ni $d_{x^2-y^2}$ pocket, suggesting that, to some approximation, it likely plays a significant role in the superconducting transition.

Weak-coupling Analysis – In order to investigate the pairing symmetry of NdNiO₂, we first consider a weak-coupling limit of the problem. Weak coupling can either be interpreted as the strictly analytically controlled perturbative limit of interactions [19–21] or, in a less restrictive meaning, as the itinerant electronic limit in which a diagrammatic, e.g. RPA treatment of interactions is adopted starting from the bare or effective electronic band structure. Such or related approaches, while less controlled than the strictly perturbative weak coupling limit, are more physically motivated, and result in qualitatively similar conclusions for pairing strengths in the system. They have enjoyed significant phenomenological success in describing unconventional superconductivity [22]. For instance, in both the weak coupling and RPA treatments of the single band Hubbard model, the dominant pairing tendency near half-filling is in the $d_{x^2-y^2}$ channel [23, 24]. A perturbative combined diagrammatic inclusion of particle-particle and particle-hole contributions could be reached by the employment of functional renormalization group [25, 26] in order to further sophisticate the RPA treatment. For the case at hand, however, the absence of magnetic order combined with the enhanced feasibility in treating three-dimensional band structures render the RPA approach most preferable at this stage of our weak coupling analysis.

In our RPA calculations, we consider onsite Hubbard intra- and inter-orbital repulsion, Hund’s coupling as well as pair hopping interactions,

$$\begin{aligned}
H_{\text{int}} = & U_{\text{Ni}} \sum_i n_{i3\uparrow} n_{i3\downarrow} + U_{\text{Nd}} \sum_{i\mu} n_{i\mu\uparrow} n_{i\mu\downarrow} \\
& + U'_{\text{Nd}} \sum_{i,\mu<\nu} n_{i\mu} n_{i\nu} + J_{\text{Nd}} \sum_{i,\mu<\nu,\sigma\sigma'} c_{i\mu\sigma}^\dagger c_{i\nu\sigma'}^\dagger c_{i\mu\sigma'} c_{i\nu\sigma} \\
& + J'_{\text{Nd}} \sum_{i,\mu\neq\nu} c_{i\mu\uparrow}^\dagger c_{i\mu\downarrow}^\dagger c_{i\nu\downarrow} c_{i\nu\uparrow}
\end{aligned} \quad (2)$$

where $n_{i\alpha} = n_{\alpha\uparrow} + n_{\alpha\downarrow}$, $\mu, \nu = 1, 2$, U_{Ni} is the Coulomb repulsion for the Ni site, thus acting on the third orbital in the notation of Eq. (1). U_{Nd} , U'_{Nd} , J_{Nd} and J'_{Nd} represent the onsite intra- and inter-orbital repulsion and the onsite Hund’s coupling and pair-hopping terms for the Nd site, respectively. For simplicity, we have chosen the same value of U for both the Nd and Ni d -orbitals. This initial choice does not fundamentally affect the effective BCS coupling that arises at order U^2 , as it is weighted by the susceptibility of each orbital. As such, the BCS couplings at low energies systematically are significantly different for Nd and Ni electrons. We use the Kanamori relations $U_{\text{Nd}} = U'_{\text{Nd}} + 2J_{\text{Nd}}$ and $J_{\text{Nd}} = J'_{\text{Nd}}$.

Fig. 3 displays the bare susceptibilities for $n = 1.0$ and

$n = 0.8$ filling, respectively. In both cases, similar to cuprates, the dominant peaks are located around the M and A points, indicating intrinsic antiferromagnetic fluctuations. These peaks get significantly enhanced upon including interactions at the RPA level. The prominent features in the orbital-resolved susceptibility are that the peaks around M and A are dominantly attributed to the Ni $d_{x^2-y^2}$ orbital while the contribution of Nd d_{xy} and d_{z^2} reaches its maximum around Γ . Based on the analysis of the susceptibility, the $d_{x^2-y^2}$ band will play the dominant role in promoting correlation phenomena, including superconductivity and, if commensurate filling of this band were reached, possible magnetic ordering.

As a systematic methodological feature, when the interaction is greater than a critical value U_c (1.1 eV in our case), the spin susceptibility within RPA diverges and indicates a spin density wave (SDW) instability. Note that as a matter of principle, U_c should be interpreted as a phenomenological parameter that does not allow an immediate quantitative connection with the bare unrenormalized interaction strength. Below U_c , superconductivity emerges triggered by spin fluctuations. We perform RPA calculations to study the possible pairing symmetries within a $40 \times 40 \times 20$ k mesh, energy window $\Delta E = 0.02$ eV around the Fermi level and inverse temperature $\beta = 50$ eV⁻¹, and have checked the convergence of pairing strength with respect to the k mesh and ΔE . With the above parameters, the numbers of the representative momentum points on the Fermi surface are 1038 and 1088 for $n = 1.0$ and $n = 0.8$, respectively. From the susceptibility, we can expect the dominant pairing state to be $d_{x^2-y^2}$ -wave (more details on the RPA are provided in the supplement [27]). As the effective low-energy interaction parameters remain as of yet largely undetermined for infinite layer nickelates, we have performed our RPA calculations within a large region of parameter space, and consistently found the dominant pairing to be unchanged, and, in particular, largely insensitive to the bare initial value U_{Nd} . The obtained pairing eigenvalues as a function of interaction strength U for $n = 1.0$ and $n = 0.8$ are displayed in Fig. 3. We find that $d_{x^2-y^2}$ pairing state is dominant, and that the gap functions are considerably smaller on the two small spherical Fermi surfaces. This is consistent with the fact that both the dominant density of states and pairing interactions reside on the Ni $d_{x^2-y^2}$ orbital.

Pairing in the t - J model – Similar to cuprates, the nickelates represent an intermediately coupled system, and it becomes important to “triangulate” the pairing problem from various limits to see if our conclusions are indeed robust. From a strong coupling perspective, the cuprates have been addressed within an effective t - J model which is either obtained from the Gutzwiller projection of a single band Hubbard model or the low-energy perturbative description of the three-band Hubbard model involving the Cu $d_{x^2-y^2}$ and the planar O $p_{x,y}$ orbitals [28]. As of yet, it is unclear whether the charge transfer gap in the nickelates [18] allows for a Zhang-Rice type Ni-O singlet complex of two holes as a suitable effective description. Still, approaching the nickelates from a related angle, we adopt the t - J model reduced to the Ni $d_{x^2-y^2}$ orbital. In

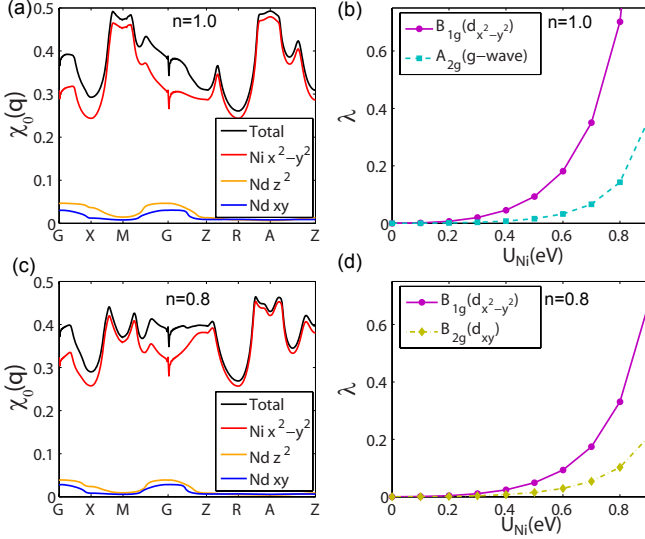


FIG. 3: Bare susceptibility (left panels) and pairing eigenvalues as a function of the interaction U_{Ni} (right panels) for electron filling $n = 1.0$ (top row) and $n = 0.8$ (bottom row), respectively. Here we adopt $U_{\text{Ni}} = U_{\text{Nd}}$ and $J_{\text{Nd}}/U_{\text{Nd}} = 0.15$.

doing so, we describe a strong coupling limit of the doped Ni $d_{x^2-y^2}$ band by constraining ourselves to the in-plane and out-of-plane antiferromagnetic couplings between the Ni spins:

$$H_J = \sum_{\langle ij \rangle} J_{ij} (\mathbf{S}_{i3} \mathbf{S}_{j3} - \frac{1}{4} n_{i3} n_{j3}), \quad (3)$$

where $\mathbf{S}_{i3} = \frac{1}{2} c_{i3\sigma}^\dagger \boldsymbol{\sigma}_{\sigma\sigma'} c_{i3\sigma'}$ is the local spin operator and n_{i3} is the local density operator for the Ni $d_{x^2-y^2}$ orbital. $\langle ij \rangle$ denotes the in-plane and out-of-plane nearest neighbor (NN). The in-plane coupling is $J_x = J_y = J_1$ and the out-of-plane coupling is J_2 . We investigate the pairing state for an extended range of doping levels. We simplify the analysis by relaxing the double-occupancy constraint on this t-J model, perform a mean-field decoupling, and solve the self-consistent gap equations [27]. We find that $d_{x^2-y^2}$ pairing is always the dominant order within extended parameter ranges of J_1 and J_2 , and that J_2 has a negligible effect on the gap. Fig. 4(a) shows the representative superconducting gap of the $d_{x^2-y^2}$ pairing as a function of doping with $J_1 = J_2 = 0.1$ eV. We find that there is a superconducting dome and the gap reaches the maximum upon 0.1 hole doping. Electron doping, by reducing the contribution of the Ni $d_{x^2-y^2}$ orbital, will significantly suppress superconductivity. Instead, beyond optimal doping, further hole doping will only slightly suppress the superconducting gap, implying to expect an extended T_c dome feature on the hole doped side. The 3D gap function of the obtained $d_{x^2-y^2}$ -wave pairing is displayed in Fig. 4(b) at 0.2 hole doping, where the gaps on the spherical Fermi surfaces from Nd atoms almost vanish. Our findings from a t-J model analysis thus are consistent with our weak-coupling analysis. *Discussion* – We have studied the infinite-layer nickelate NdNiO₂ and have found that the dominant pairing instabil-

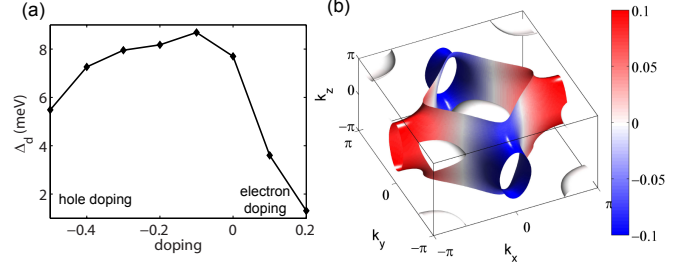


FIG. 4: (a) The $d_{x^2-y^2}$ -wave gap as a function doping with $J_1 = J_2 = 0.1$ eV. Positive (negative) values relate to electron (hole) doping. (b) Superconducting gap for $d_{x^2-y^2}$ -wave pairing. In the calculations, a k mesh of $100 \times 100 \times 50$ has been adopted.

ity is in the $d_{x^2-y^2}$ channel, which places this system in close analogy with cuprate superconductors. As a consequence of the pairing symmetry, we expect nodes on the Fermi surface, the evidence for which can be found in low temperature heat capacity [29], penetration depth [30] measurements, quasiparticle interference studies [31], and more directly, from phase-sensitive studies [32, 33].

In the future, it will be interesting to study the role of the Nd itinerant electrons in conjunction with the local moments of the Ni sites. It is thus tempting to invoke the analogy with heavy fermion systems, and to view the physics of the infinite layer nickelate from the vantage point of the Kondo lattice. In this context, it is reasonable to presume that the effect of strontium doping involves more complex phenomena than a simple rigid shift of the Fermi level. Furthermore, even though an electronically mediated pairing mechanism may appear likely judging from the current experimental evidence, the impact of electron-phonon coupling will be vital to gaining a deeper understanding of the material [34]. We wish to pursue such questions in future studies.

Acknowledgments - The work in Würzburg is funded by the Deutsche Forschungsgemeinschaft (DFG, German Research Foundation) through Project-ID 258499086 - SFB 1170 and through the Würzburg-Dresden Cluster of Excellence on Complexity and Topology in Quantum Matter – *ct.qmat* Project-ID 39085490 - EXC 2147. H.Y.H. and S.R. are supported by the DOE Office of Basic Energy Sciences, contract DEAC02-76SF00515. We gratefully acknowledge the Gauss Centre for Supercomputing e.V. (www.gauss-centre.eu) for funding this project by providing computing time on the GCS Supercomputer SuperMUC at Leibniz Supercomputing Centre (www.lrz.de).

Note added - After completion of our work, we learned about an independent study of electronic structure and pairing instabilities in the infinite layer nickelate (Ref. [35]). This study makes use of a variant of the RPA method (FLEX) and finds similar conclusions for pairing.

-
- * These authors equally contributed to the work.; Electronic address: xianxinwu@gmail.com
- † These authors equally contributed to the work.
- ‡ Electronic address: sraghu@stanford.edu
- § Electronic address: rthomale@physik.uni-wuerzburg.de
- [1] D. Li, K. Lee, B. Y. Wang, M. Osada, S. Crossley, H. R. Lee, Y. Cui, Y. Hikita, and H. Y. Hwang, *Nature* **572**, 624 (2019).
 - [2] P. A. Lee, N. Nagaosa, and X.-G. Wen, *Rev. Mod. Phys.* **78**, 17 (2006).
 - [3] B. Keimer, S. A. Kivelson, M. R. Norman, S. Uchida, and J. Zaanen, *Nature* **518**, 179 (2015).
 - [4] Y. Maeno, H. Hashimoto, K. Yoshida, S. Nishizaki, T. Fujita, J. Bednorz, and F. Lichtenberg, *Nature* **372**, 532 (1994).
 - [5] J. Chaloupka and G. Khaliullin, *Physical Review Letters* **100**, 016404 (2008).
 - [6] Y. K. Kim, N. Sung, J. Denlinger, and B. Kim, *Nature Physics* **12**, 37 (2016).
 - [7] V. I. Anisimov, D. Bukhvalov, and T. M. Rice, *Phys. Rev. B* **59**, 7901 (1999).
 - [8] K.-W. Lee and W. E. Pickett, *Phys. Rev. B* **70**, 165109 (2004).
 - [9] P. Hansmann, X. Yang, A. Toschi, G. Khaliullin, O. K. Andersen, and K. Held, *Phys. Rev. Lett.* **103**, 016401 (2009).
 - [10] M. Hayward, M. Green, M. Rosseinsky, and J. Sloan, *Journal of the American Chemical Society* **121**, 8843 (1999).
 - [11] M. Hayward and M. Rosseinsky, *Solid State Sciences* **5**, 839 (2003).
 - [12] G. Kotliar and J. Liu, *Phys. Rev. B* **38**, 5142 (1988).
 - [13] G. Kresse and J. Furthmüller, *Phys. Rev. B* **54**, 11169 (1996).
 - [14] G. Kresse and D. Joubert, *Phys. Rev. B* **59**, 1758 (1999).
 - [15] P. E. Blöchl, *Phys. Rev. B* **50**, 17953 (1994).
 - [16] J. P. Perdew, K. Burke, and M. Ernzerhof, *Phys. Rev. Lett.* **77**, 3865 (1996).
 - [17] A. A. Mostofi, J. R. Yates, Y.-S. Lee, I. Souza, D. Vanderbilt, and N. Marzari, *Comput. Phys. Commun.* **178**, 685 (2008).
 - [18] A. S. Botana and M. R. Norman, *arXiv preprint arXiv:1908.10946* (2019).
 - [19] W. Kohn and J. Luttinger, *Phys. Rev. Lett.* **15**, 524 (1965).
 - [20] S. Raghu, S. A. Kivelson, and D. J. Scalapino, *Phys. Rev. B* **81**, 224505 (2010).
 - [21] W. Cho, R. Thomale, S. Raghu, and S. A. Kivelson, *Phys. Rev. B* **88**, 064505 (2013).
 - [22] D. J. Scalapino, *Rev. Mod. Phys.* **84**, 1383 (2012).
 - [23] D. J. Scalapino, E. Loh, and J. E. Hirsch, *Phys. Rev. B* **34**, 8190 (1986).
 - [24] K. Miyake, S. Schmitt-Rink, and C. M. Varma, *Phys. Rev. B* **34**, 6554 (1986).
 - [25] W. Metzner, M. Salmhofer, C. Honerkamp, V. Meden, and K. Schönhammer, *Rev. Mod. Phys.* **84**, 299 (2012).
 - [26] C. Platt, W. Hanke, and R. Thomale, *Advances in Physics* **62**, 453 (2013).
 - [27] see Supplemental Material [url].
 - [28] F. C. Zhang and T. M. Rice, *Phys. Rev. B* **37**, 3759 (1988).
 - [29] K. A. Moler, A. Kapitulnik, D. J. Baar, R. Liang, and W. N. Hardy, *Journal of Physics and Chemistry of Solids* **56**, 1899 (1995), proceedings of the Conference on Spectroscopies in Novel Superconductors.
 - [30] W. N. Hardy, D. A. Bonn, D. C. Morgan, R. Liang, and K. Zhang, *Phys. Rev. Lett.* **70**, 3999 (1993).
 - [31] J. E. Hoffman, K. McElroy, D.-H. Lee, K. M. Lang, H. Eisaki, S. Uchida, and J. C. Davis, *Science* **297**, 1148 (2002).
 - [32] D. J. Van Harlingen, *Rev. Mod. Phys.* **67**, 515 (1995).

- [33] C. C. Tsuei and J. R. Kirtley, *Rev. Mod. Phys.* **72**, 969 (2000).
- [34] Y. Nomura, M. Hirayama, T. Tadano, Y. Yoshimoto, K. Nakamura and R. Arita, *Phys. Rev. B* **100**, 205138 (2019).
- [35] H. Sakakibara, H. Usui, K. Suzuki, T. Kotani, H. Aoki, and K. Kuroki, *arXiv e-prints arXiv:1909.00060* (2019).

DFT bands and Tight-binding model

Fig.S5 shows the DFT band structure with a large energy window and the band structures in $k_z = 0$ and $k_z = \pi$ plane. In the $k_z = \pi$ plane, the van Hove singularity point at R is extremely close to the Fermi level. To reproduce the DFT band structure we construct a tight-binding model, which was given the main text. The adopted three-band tight binding Hamiltonian is given in Eq.1. The matrix elements in the Hamiltonian $h(\mathbf{k})$ matrix are given by,

$$h_{11}(\mathbf{k}) = \epsilon_1 - \mu + 2t_{11}^x(\cos k_x + \cos k_y) + 4t_{11}^{xy}\cos k_x\cos k_y + 2t_{11}^{xx}(\cos 2k_x + \cos 2k_y) + 4t_{11}^{xy}(\cos 2k_x\cos k_y + \cos k_x\cos 2k_y) + 2t_{11}^{zz}\cos k_z + 2t_{11}^{zz}\cos 2k_z + 4t_{11}^{xz}\cos k_z(\cos k_x + \cos k_y) + 8t_{11}^{xyz}\cos k_x\cos k_y\cos k_z \quad (\text{S4})$$

$$h_{22}(\mathbf{k}) = \epsilon_2 - \mu + 2t_{22}^x(\cos k_x + \cos k_y) + 4t_{22}^{xy}\cos k_x\cos k_y + 2t_{22}^{xx}(\cos 2k_x + \cos 2k_y) + 4t_{22}^{xy}(\cos 2k_x\cos k_y + \cos k_x\cos 2k_y) + 2t_{22}^{zz}\cos k_z + 2t_{22}^{zz}\cos 2k_z + 4t_{22}^{xz}\cos k_z(\cos k_x + \cos k_y) + 8t_{22}^{xyz}\cos k_x\cos k_y\cos k_z + 8t_{22}^{xxz}\cos k_z(\cos 2k_x + \cos 2k_y) + 8t_{22}^{xyx}\cos k_z(\cos 2k_x\cos k_y + \cos k_x\cos 2k_y) + 8t_{22}^{xyx}\cos k_z(\cos 2k_x\cos k_y + \cos k_x\cos 2k_y) + 2t_{22}^{xxx}(\cos 3k_x + \cos 3k_y) \quad (\text{S5})$$

$$h_{33}(\mathbf{k}) = \epsilon_3 - \mu + 2t_{33}^x(\cos k_x + \cos k_y) + 4t_{33}^{xy}\cos k_x\cos k_y + 2t_{33}^{xx}(\cos 2k_x + \cos 2k_y) + 4t_{33}^{xy}(\cos 2k_x\cos k_y + \cos k_x\cos 2k_y) + 4t_{33}^{xyy}\cos 2k_x\cos 2k_y + 2t_{33}^{zz}\cos k_z + 2t_{33}^{zz}\cos 2k_z + 4t_{33}^{xz}\cos k_z(\cos k_x + \cos k_y) + 8t_{33}^{xyz}\cos k_x\cos k_y\cos k_z \quad (\text{S6})$$

$$h_{12}(\mathbf{k}) = -4t_{12}^{xy}\sin k_x\sin k_y - 8t_{12}^{xyz}\sin k_x\sin k_y\cos k_z - 8t_{12}^{xyz}\sin k_x\sin k_y\cos 2k_z \quad (\text{S7})$$

$$h_{13}(\mathbf{k}) = -8t_{13}^{xyz}\cos k_z/2(\sin 3k_x/2\sin k_y/2 - \sin k_x/2\sin 3k_y/2) \quad (\text{S8})$$

$$h_{23}(\mathbf{k}) = 8t_{23}^{xyz}\cos k_z/2(\cos 3k_x/2\cos k_y/2 - \cos k_x/2\cos 3k_y/2) \quad (\text{S9})$$

The corresponding tight binding parameters are specified in unit of eV as,

$$\epsilon_1 = 8.9506, \quad \epsilon_2 = 9.0277, \quad \epsilon_3 = 6.8979, \quad (\text{S10})$$

$$t_{11}^x = -0.3870, \quad t_{11}^{xy} = 0, \quad t_{11}^{xx} = 0.034, \quad t_{11}^z = -0.8591, \quad t_{11}^{xz} = 0.0107, \quad t_{11}^{xyz} = 0.025, \quad t_{11}^{zz} = 0.0904, \quad (\text{S11})$$

$$t_{22}^x = 0.3202, \quad t_{22}^{xy} = -0.0467, \quad t_{22}^{xx} = 0.0367, \quad t_{22}^z = 0.3216, \quad t_{22}^{xz} = -0.1438, \quad t_{22}^{xyz} = 0.0496, \quad t_{22}^{zz} = -0.0327, \quad t_{22}^{zzz} = -0.0209, \quad t_{22}^{xyx} = -0.0198, \quad t_{22}^{xyx} = 0.0164, \quad t_{22}^{xxx} = 0.012 \quad (\text{S12})$$

$$t_{12}^{xy} = 0.0798, \quad t_{12}^{xyz} = -0.0669, \quad t_{12}^{xyz} = 0.0094, \quad (\text{S13})$$

$$t_{33}^x = -0.3761, \quad t_{33}^{xy} = 0.0844, \quad t_{33}^{xx} = -0.0414, \quad t_{33}^{xyz} = -0.0043, \quad t_{33}^{xyy} = 0.003, \quad t_{33}^z = -0.0368, \quad t_{33}^{zz} = -0.0019, \quad t_{33}^{zzz} = 0.0117, \quad t_{33}^{zz} = 0.008, \quad (\text{S14})$$

$$t_{13}^{xyz} = 0.0219, \quad t_{23}^{xyz} = -0.0139. \quad (\text{S15})$$

With $\mu = 6.5814$ eV, the occupation number is 1.0. With 0.2 hole doping, the corresponding chemical potential is $\mu = 6.4614$ eV. The band structures from the tight-binding model with the above parameters are displayed in Fig.S6, which are in good agreement with DFT calculations.

weak-coupling limit: RPA approach

The adopted interactions are given in the main text. The bare susceptibility is define as,

$$\chi_{l_1 l_2 l_3 l_4}^0(\mathbf{q}, \tau) = \frac{1}{N} \sum_{\mathbf{k} \mathbf{k}'} \langle T_\tau c_{l_3 \sigma}^\dagger(\mathbf{k} + \mathbf{q}, \tau) c_{l_4 \sigma}(\mathbf{k}, \tau) c_{l_2 \sigma}^\dagger(\mathbf{k}' - \mathbf{q}, 0) c_{l_1 \sigma}(\mathbf{k}', 0) \rangle_0. \quad (\text{S16})$$

where l_i is the orbital indices. The bare susceptibility in momentum-frequency is,

$$\chi_{l_1 l_2 l_3 l_4}^0(\mathbf{q}, i\omega_n) = -\frac{1}{N} \sum_{\mathbf{k} \mu \nu} a_{\mu}^{l_4}(\mathbf{k}) a_{\mu}^{l_2*}(\mathbf{k}) a_{\nu}^{l_1}(\mathbf{k} + \mathbf{q}) a_{\nu}^{l_3*}(\mathbf{k} + \mathbf{q}) \frac{n_F(E_{\mu}(\mathbf{k})) - n_F(E_{\nu}(\mathbf{k} + \mathbf{q}))}{i\omega_n + E_{\mu}(\mathbf{k}) - E_{\nu}(\mathbf{k} + \mathbf{q})}. \quad (\text{S17})$$

where μ/ν is the band index, $n_F(\epsilon)$ is the Fermi distribution function, $a_{\mu}^{l_i}(\mathbf{k})$ is the l_i -th component of the eigenvector for band μ resulting from the diagonalization of the tight-binding Hamiltonian H_{TB} and $E_{\mu}(\mathbf{k})$ is the eigenvalue of band μ . The interacting spin susceptibility and charge susceptibility in RPA level are given by,

$$\chi_1^{RPA}(\mathbf{q}) = [1 - \chi_0(\mathbf{q})U^s(\mathbf{q})]^{-1}\chi_0(\mathbf{q}), \quad (\text{S18})$$

$$\chi_0^{RPA}(\mathbf{q}) = [1 + \chi_0(\mathbf{q})U^c(\mathbf{q})]^{-1}\chi_0(\mathbf{q}), \quad (\text{S19})$$

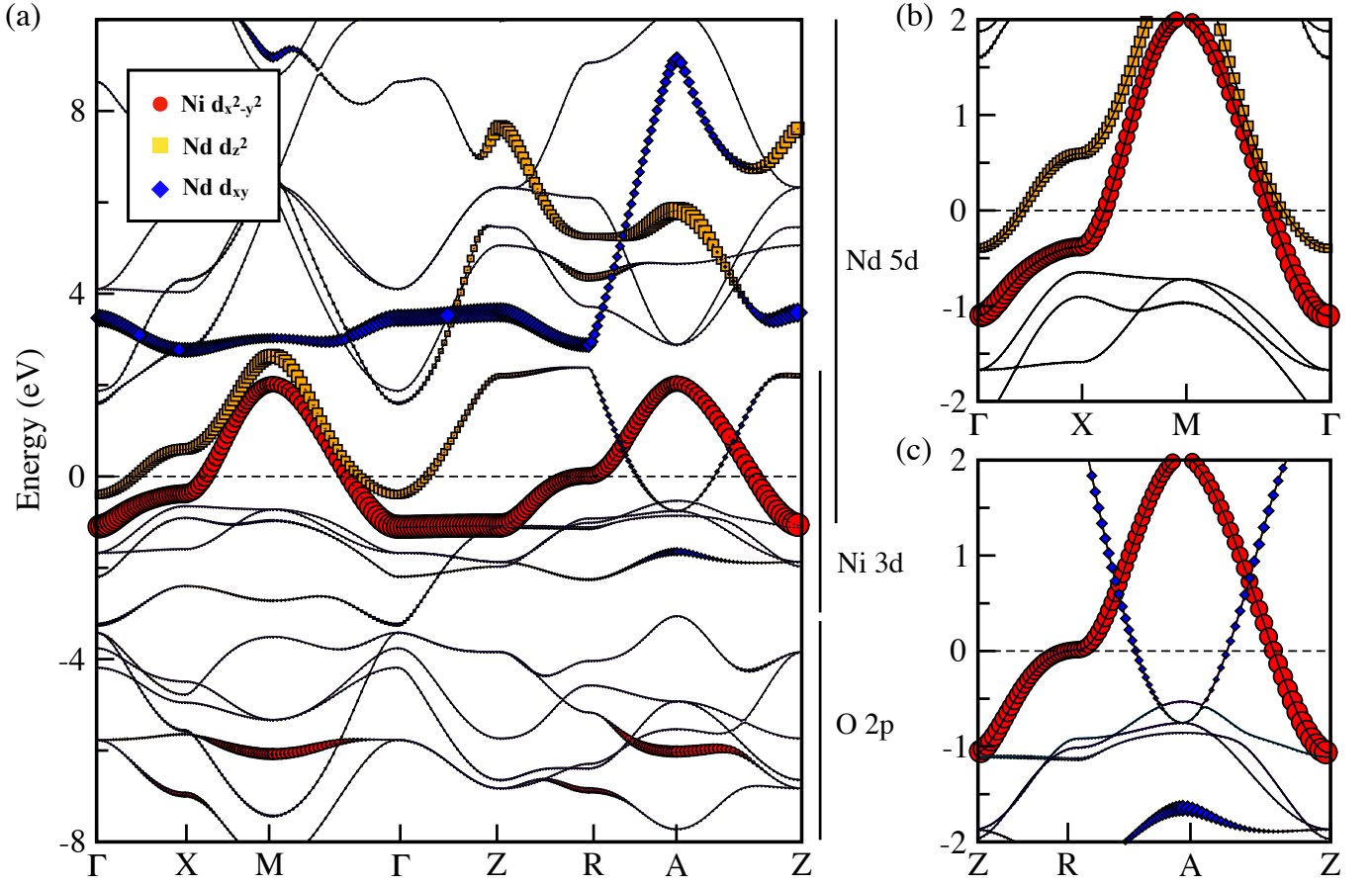


FIG. S5: (a) First-principles band structure of NdNiO_2 with lattice parameters forced by the commensuration to the SrTiO_3 substrate. The lateral bars qualitatively identify the range of energy extension of the relative atomic contributions. A sizable hybridization between $\text{Ni } 3d$ and $\text{Nd } 5d$ states is expected close the Fermi level. The red, yellow and blue symbols emphasize the relevant orbitals that contribute to the low-energy description. (b-c) Enlarged views of the band structure around the Fermi level at (b) $k_z = 0$ and (c) $k_z = \pi/c$, respectively

where U^s, U^c are the interaction matrices are,

$$U_{\alpha l_1, \alpha l_2, \alpha l_3, \alpha l_4}^s(\mathbf{q}) = \begin{cases} U_\alpha & l_1 = l_2 = l_3 = l_4, \\ U'_\alpha & l_1 = l_3 \neq l_2 = l_4, \\ J_\alpha & l_1 = l_2 \neq l_3 = l_4, \\ J'_\alpha & l_1 = l_4 \neq l_2 = l_3, \end{cases} \quad (\text{S20})$$

$$U_{\alpha l_1, \alpha l_2; \alpha l_3, \alpha l_4}^c(\mathbf{q}) = \begin{cases} U_\alpha & l_1 = l_2 = l_3 = l_4, \\ -U'_\alpha + 2J_\alpha & l_1 = l_3 \neq l_2 = l_4, \\ 2U'_\alpha - J_\alpha & l_1 = l_2 \neq l_3 = l_4, \\ J'_\alpha & l_1 = l_4 \neq l_2 = l_3, \end{cases} \quad (\text{S21})$$

Here α is the sublattice index. For Nd site with $\alpha = A$, the interactions parameters are: $U_A = U$, $U'_A = U'$, $J_A = J$ and $J'_A = J'$. For Ni site with $\alpha = B$, the only non-vanishing interaction parameter is $U_B = U_3$. We plot the susceptibility in the main text, which is defined as $\chi_{0/RPA} = \frac{1}{2} \sum_{l_1, l_2} \chi_{l_1 l_1; l_2 l_2}^{0/RPA}(\mathbf{q}, 0)$. We also calculate the largest eigenvalues of the susceptibility matrix in momentum space (not shown), which is very similar to χ_0 . The effective interaction obtained in the RPA approximation is,

$$V_{eff} = \sum_{ij, \mathbf{k}\mathbf{k}'} \Gamma_{ij}(\mathbf{k}, \mathbf{k}') c_{i\mathbf{k}\uparrow}^\dagger c_{i-\mathbf{k}\downarrow}^\dagger c_{j-\mathbf{k}'\downarrow} c_{j\mathbf{k}'\uparrow} \quad (\text{S22})$$

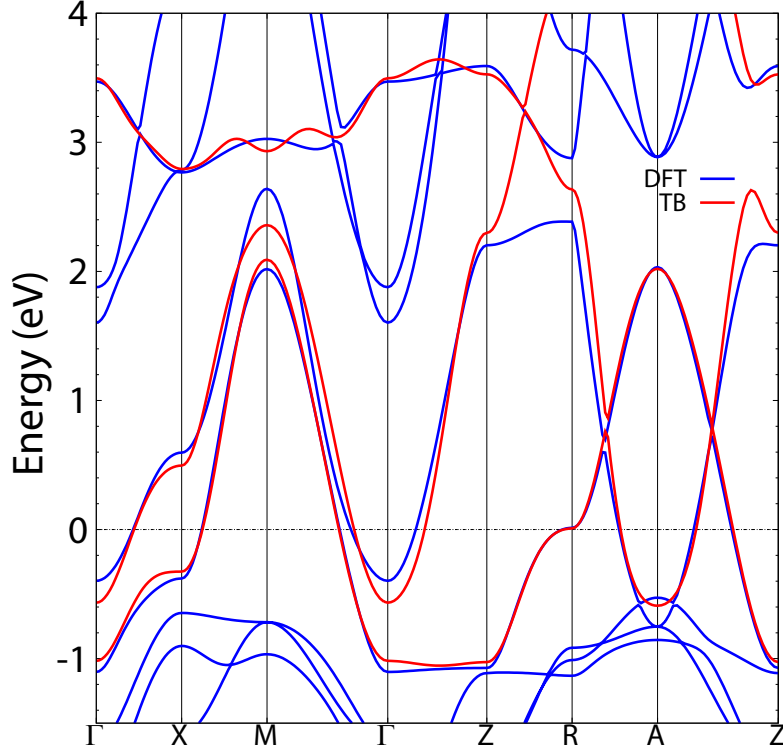


FIG. S6: Band structures from DFT (blue lines) and tight-binding model (red lines).

where the momenta \mathbf{k} and \mathbf{k}' are restricted to different FS C_i with $\mathbf{k} \in C_i$ and $\mathbf{k}' \in C_j$ and $\Gamma_{ij}(\mathbf{k}, \mathbf{k}')$ is the pairing scattering vertex in the singlet channel[S1]. The pairing vertex is,

$$\Gamma_{ij}(\mathbf{k}, \mathbf{k}') = \sum_{l_1 l_2 l_3 l_4} a_{v_i}^{l_2,*}(\mathbf{k}) a_{v_i}^{l_3,*}(-\mathbf{k}) \text{Re}[\Gamma_{l_1 l_2 l_3 l_4}(\mathbf{k}, \mathbf{k}', \omega = 0)] a_{v_j}^{l_1}(\mathbf{k}') a_{v_j}^{l_4}(-\mathbf{k}'), \quad (\text{S23})$$

where a_v^l (orbital index l and band index v) is the component of the eigenvectors from the diagonalization of the tight binding Hamiltonian. The orbital vertex function $\Gamma_{l_1 l_2 l_3 l_4}$ for the singlet channel and triplet channel in the fluctuation exchange formulation[S1–S5] are given by,

$$\Gamma_{l_1 l_2 l_3 l_4}^S(\mathbf{k}, \mathbf{k}', \omega) = [\frac{3}{2} \bar{U}^s \chi_1^{RPA}(\mathbf{k} - \mathbf{k}', \omega) \bar{U}^s + \frac{1}{2} \bar{U}^s - \frac{1}{2} \bar{U}^c \chi_0^{RPA}(\mathbf{k} - \mathbf{k}', \omega) \bar{U}^c + \frac{1}{2} \bar{U}^c]_{l_1 l_2 l_3 l_4}, \quad (\text{S24})$$

$$\Gamma_{l_1 l_2 l_3 l_4}^T(\mathbf{k}, \mathbf{k}', \omega) = [-\frac{1}{2} \bar{U}^s \chi_1^{RPA}(\mathbf{k} - \mathbf{k}', \omega) \bar{U}^s + \frac{1}{2} \bar{U}^s - \frac{1}{2} \bar{U}^c \chi_0^{RPA}(\mathbf{k} - \mathbf{k}', \omega) \bar{U}^c + \frac{1}{2} \bar{U}^c]_{l_1 l_2 l_3 l_4}, \quad (\text{S25})$$

where $\bar{U}^{s/c} = U^{s/c}(\mathbf{k} - \mathbf{k}')$. The χ_0^{RPA} describes the charge fluctuation contribution and the χ_1^{RPA} the spin fluctuation contribution. For a given gap function $\Delta(\mathbf{k})$, the pairing strength functional is,

$$\lambda[\Delta(\mathbf{k})] = - \frac{\sum_{ij} \oint_{C_i} \frac{dk_{\parallel}}{v_F(\mathbf{k})} \oint_{C_j} \frac{dk'_{\parallel}}{v_F(\mathbf{k}')} \Delta(\mathbf{k}) \Gamma_{ij}(\mathbf{k}, \mathbf{k}') \Delta(\mathbf{k}')}{V_G \sum_i \oint_{C_i} \frac{dk_{\parallel}}{v_F(\mathbf{k})} [\Delta(\mathbf{k})]^2}, \quad (\text{S26})$$

where $v_F(\mathbf{k}) = |\nabla_{\mathbf{k}} E_i(\mathbf{k})|$ is the Fermi velocity on a given fermi surface sheet C_i and V_G is the volume of the Brillouin zone. From the stationary condition we find the following eigenvalue problem,

$$- \sum_j \oint_{C_j} \frac{dk'_{\parallel}}{V_G v_F(\mathbf{k}')} \Gamma_{ij}(\mathbf{k}, \mathbf{k}') \Delta_{\alpha}(\mathbf{k}') = \lambda_{\alpha} \Delta_{\alpha}(\mathbf{k}), \quad (\text{S27})$$

where the interaction Γ_{ij} is the symmetric (antisymmetric) part of the full interaction in singlet (triplet) channel. The leading eigenfunction $\Delta_{\alpha}(\mathbf{k})$ and eigenvalue λ_{α} are obtained from the above equation. In the calculation, we treat those k points, whose energies lie within a small energy window ΔE around the Fermi level, as effective k points in the pairing vertex function. We have checked the convergence of λ with respect to k -mesh and ΔE (with denser $50 \times 50 \times 30$ k mesh and $\Delta E = 0.01$ eV).

pairing from the t-J model

In the strong-coupling limit, similar to cuprate, we consider the inplane and outplane antiferromagnetic couplings between the spin of Ni $d_{x^2-y^2}$ orbital,

$$H_J = \sum_{\langle ij \rangle} J_{ij} (\mathbf{S}_{i3} \mathbf{S}_{j3} - \frac{1}{4} n_{i3} n_{j3}) \quad (\text{S28})$$

where $\mathbf{S}_{i3} = \frac{1}{2} c_{i3\sigma}^\dagger \boldsymbol{\sigma}_{\sigma\sigma'} c_{i3\sigma'}$ is the local spin operator and n_{i3} is the local density operator for Ni $d_{x^2-y^2}$ orbital. $\langle ij \rangle$ denotes the inplane and outplane nearest neighbor (NN). The inplane coupling is $J_x = J_y = J_1$ and the outplane coupling is J_z . By performing the Fourier transformation, H_J in momentum space reads

$$H_J = \sum_{\mathbf{k}, \mathbf{k}'} V_{\mathbf{k}, \mathbf{k}'} c_{\mathbf{k}3\uparrow}^\dagger c_{-\mathbf{k}3\downarrow}^\dagger c_{-\mathbf{k}'3\downarrow} c_{\mathbf{k}'3\uparrow}, \quad (\text{S29})$$

with $V_{\mathbf{k}, \mathbf{k}'} = -\frac{2J_1}{N} \sum_{\pm} (\cos k_x \pm \cos k_y) (\cos k'_x \pm \cos k'_y) - \frac{2J_2}{N} \cos k_z \cos k'_z$. Here we investigate the pairing state for doped system and neglect the no-double-occupance constraint on this $t - J$ model and perform a mean-field decoupling, similar to the iron based superconductors [S6]. With this, the total Hamiltonian can be written as,

$$H_{MF} = \sum_{\mathbf{k}} \Psi_{\mathbf{k}}^\dagger A(\mathbf{k}) \Psi_{\mathbf{k}} + \frac{N}{2J_1} \sum_{\nu=s,d} |\Delta_\nu|^2 + \frac{N}{2J_2} |\Delta_z|^2, \quad (\text{S30})$$

$$A(\mathbf{k}) = \begin{pmatrix} h(\mathbf{k}) & \Delta_{\uparrow\downarrow}(\mathbf{k}) \\ \Delta_{\uparrow\downarrow}^\dagger(\mathbf{k}) & -h^*(-\mathbf{k}) \end{pmatrix},$$

$$\Delta_{\uparrow\downarrow}(\mathbf{k}) = \begin{pmatrix} 0 & \\ & 0 \\ & & \Delta_3(\mathbf{k}) \end{pmatrix}, \quad (\text{S31})$$

where $\Psi_{\mathbf{k}}^\dagger = (\psi_{\mathbf{k}\uparrow}^\dagger, \psi_{-\mathbf{k}\downarrow}^T)$, $\Delta_3(\mathbf{k}) = \Delta_s(\cos k_x + \cos k_y) + \Delta_d(\cos k_x - \cos k_y) + \Delta_z \cos k_z$, and

$$\Delta_{s/d} = -\frac{2J_1}{N} \sum_{\mathbf{k}'} d_{\mathbf{k}'\uparrow} (\cos k'_x \pm \cos k'_y), \quad (\text{S32})$$

$$\Delta_z = -\frac{2J_2}{N} \sum_{\mathbf{k}'} d_{\mathbf{k}'\uparrow} \cos k'_z, \quad (\text{S33})$$

with $d_{\mathbf{k}'\uparrow} = \langle c_{-\mathbf{k}'3\downarrow} c_{\mathbf{k}'3\uparrow} \rangle$. $A(\mathbf{k})$ can be diagonalized by a unitary transformation $U_{\mathbf{k}}$ with the Bogoliubov quasiparticle eigenvalues $E_{m+3} = -E_m$ with $m = 1, 2, 3$. The self-consistent gap equations are

$$\Delta_{s/d} = -\frac{2J_1}{N} \sum_{\mathbf{k}, m} (\cos k_x \pm \cos k_y) U_{6,m}^*(\mathbf{k}) U_{3,m}(\mathbf{k}) F[E_m(\mathbf{k})]$$

$$\Delta_z = -\frac{2J_2}{N} \sum_{\mathbf{k}, m} \cos k_z U_{6,m}^*(\mathbf{k}) U_{3,m}(\mathbf{k}) F[E_m(\mathbf{k})] \quad (\text{S34})$$

where $F[E]$ is Fermi-Dirac distribution function, $F[E] = 1/(1 + e^{E/k_B T})$. The above equations can be solved self-consistently, varying the doping and the value of J_1, J_2 . For $n = 1.0$ and $n = 0.8$, the obtained $d_{x^2-y^2}$ gap and ground-state energy as a function of J_1 ($J_1 = J_2$) are given in Fig. S7 (a) and (b). With J_1 being larger than 0.05, the $d_{x^2-y^2}$ superconducting gap and ground-state energy increases abruptly. With $J_1 = J_2 = 0.1$, Fig. 4 in the main text shows the superconducting gap as a function of doping. We find that electron doping will significantly suppress superconductivity and the gap reaches the maximum with 0.1 hole doping. Further hole doping will suppress the gap size. The 3D gap function of $d_{x^2-y^2}$ -wave pairing is shown in Fig. 4 (b) for $n = 0.8$, where the gap on the spherical Fermi surfaces almost vanishes. These are consistent with the RPA calculations.

* These authors equally contributed to the work.; Electronic address: xianxinwu@gmail.com

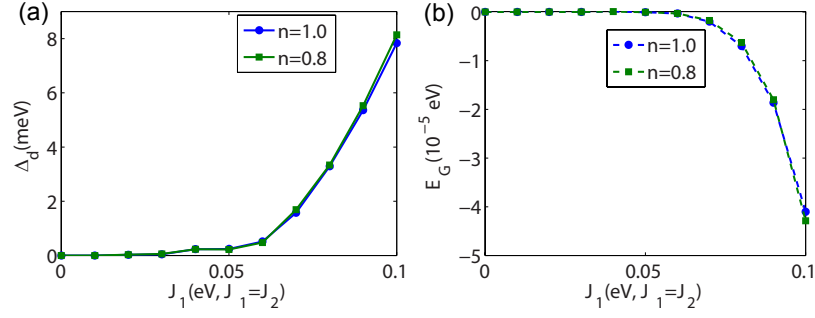


FIG. S7: (a) The gap function of $d_{x^2-y^2}$ pairing state as a function of J_1 for $n = 1.0$ and $n = 0.8$. (b) The ground-state energy relative to the normal state as a function of J_1 for $n = 1.0$ and $n = 0.8$. In the calculations, a k mesh of $100 \times 100 \times 50$ is adopted.

[†] These authors equally contributed to the work.

[‡] Electronic address: sraghu@stanford.edu

[§] Electronic address: rthomale@physik.uni-wuerzburg.de

[S1] A. F. Kemper, T. A. Maier, S. Graser, H.-P. Cheng, P. J. Hirschfeld, and D. J. Scalapino, New J. Phys. **12**, 073030 (2010).

[S2] N. E. Bickers, D. J. Scalapino, and S. R. White, Phys. Rev. Lett. **62**, 961 (1989).

[S3] K. Kubo, Phys. Rev. B **75**, 224509 (2007).

[S4] X. Wu, J. Yuan, Y. Liang, H. Fan, and J. Hu, EPL (Europhysics Letters) **108**, 27006 (2014).

[S5] X. Wu, F. Yang, C. Le, H. Fan, and J. Hu, Phys. Rev. B **92**, 104511 (2015).

[S6] K. Seo, B. A. Bernevig, and J. Hu, Phys. Rev. Lett. **101**, 206404 (2008).